tion patterns were observed on different cooling cycles. With more oblate plasmas, the same pattern was observed each time. A very oblate plasma resembles the planar geometry considered by Dubin and O'Neil (*9*, *10*), in which a stack of bcc (110) planes was predicted to have the lowest energy when there are about 60 or more planes. For some cases with fewer planes, a stack of fcc (111) planes has lower energy. In a time-resolved diffraction pattern from a plasma having $\alpha = 0.38$ (Fig. 6), the most intense diffraction spots form a rectangular array, consistent with a bcc lattice oriented along a ⟨110⟩ direction, that is, a stack of (110) planes. Weaker diffraction spots, forming a hexagon, are also seen. These appear at the lowest temperatures. The expected positions of the spots for the {220} Bragg reflections of an fcc lattice oriented along a ⟨111⟩ direction, that is, a stack of (111) planes, are at the vertices of the hexagon overlay. An ideal hexagonal close-packed lattice, oriented along the [001] direction, would generate the same hexagonal spot pattern. However, it would also generate another hexagonal spot pattern at a smaller radius, which is not observed.

Simulations of ion plasmas show hexagonal patterns resembling fcc (111) planes on the layers nearest the surface (*7*). The hexagonal diffraction pattern in Fig. 6 could be the result of scattering from surface layers, and the rectangular pattern could result from scattering from the central region. Some spots in Fig. 6 do not match either the rectangular grid or a hexagonal lattice. They may be due to scattering from a transition region that is neither bcc nor fcc. Further examination of oblate plasmas with different thicknesses may enable the transition from surface-dominated structure to bulk behavior in a finite, strongly coupled OCP to be studied.

REFERENCES AND NOTES

1. S. Ichimaru, *Rev. Mod. Phys.* **54**, 1017 (1982).
2. H. M. Van Horn, *Science* **252**, 384 (1991).
3. E. L. Pollock and J. P. Hansen, *Phys. Rev. A* **8**, 3110 (1973); W. L. Slattery, G. D. Doolen, H. E. DeWitt, *ibid.* **21**, 2087 (1980); *ibid.* **26**, 2255 (1982); S. Ogata and S. Ichimaru, *ibid.* **36**, 5451 (1987); G. S. Stringfellow and H. E. DeWitt, *ibid.* **41**, 1105 (1990); D. H. E. Dubin, *ibid.* **42**, 4972 (1990).
4. R. C. Davidson, *Physics of Nonneutral Plasmas* (Addison-Wesley, Redwood City, CA, 1990), chap. 3.3.
5. J. H. Malmberg and T. M. O'Neil, *Phys. Rev. Lett.* **39**, 1333 (1977).
6. J. J. Bollinger, D. J. Wineland, D. H. E. Dubin, *Phys. Plasmas* **1**, 1403 (1994).
7. A. Rahman and J. P. Schiffer, *Phys. Rev. Lett.* **57**, 1133 (1986); H. Totsuji, in *Strongly Coupled Plasma Physics*, F. J. Rogers and H. E. DeWitt, Eds. (Plenum, New York, 1987), p. 19; D. H. E. Dubin and T. M. O'Neil, *Phys. Rev. Lett.* **60**, 511 (1988); J. P. Schiffer, *ibid.* **61**, 1843 (1988); R. W. Hasse and V. V. Avilov, *Phys. Rev. A* **44**, 4506 (1991); J. P. Schiffer, in *Non-neutral Plasma Physics II*, F. Fajans and D. H. E. Dubin, Eds. (American Institute of Physics (AIP) Conference Proceedings 331, AIP Press, New York, 1995), p. 191.
8. S. L. Gilbert, J. J. Bollinger, D. J. Wineland, *Phys. Rev. Lett.* **60**, 2022 (1988).
9. D. H. E. Dubin, *Phys. Rev. A* **40**, 1140 (1989).
10. ______ and T. M. O'Neil, in *Strongly Coupled Plasma Physics*, S. Ichimaru, Ed. (Elsevier, Amsterdam, 1990), p. 189.
11. G. Birkl, S. Kassner, H. Walther, *Nature* **357**, 310 (1992).
12. M. Drewsen, C. Brodersen, L. Hornekær, J. S. Hangst, J. P. Schiffer, in preparation.
13. J. N. Tan, J. J. Bollinger, B. Jelenković, D. J. Wineland, *Phys. Rev. Lett.* **72**, 4198 (1995).
14. A preliminary report of the time-resolved detection has appeared [J. N. Tan, J. J. Bollinger, B. Jelenković, W. M. Itano, D. J. Wineland, in *Physics of Strongly Coupled Plasmas*, Proceedings of the International Conference, Binz, Germany, W. D. Kraeft and M. Schlanges, Eds. (World Scientific, Singapore, 1996), p. 387].
15. J. J. Bollinger and D. J. Wineland, *Phys. Rev. Lett.* **53**, 348 (1984).
16. L. R. Brewer *et al.*, *Phys. Rev. A* **38**, 859 (1988).
17. X.-P. Huang, F. Anderegg, E. M. Hollman, C. F. Driscoll, T. M. O'Neil, *Phys. Rev. Lett.* **78**, 875 (1997).
18. X.-P. Huang, J. J. Bollinger, T. B. Mitchell, W. M. Itano, *ibid.* **80**, 73 (1998).
19. The notation refers to the conventional cubic unit cells for the bcc and fcc lattices. A lattice plane specified by Miller indices h, k, and ℓ is denoted by $(hk\ell)$; a direction specified by components n_1, n_2, and n_3 is denoted by $[n_1n_2n_3]$; a set of planes that are equivalent by symmetry is denoted by $\{hk\ell\}$; and a set of directions that are equivalent by symmetry is denoted by $\langle n_1n_2n_3\rangle$. See, for example, N. W. Ashcroft and N. D. Mermin, *Solid State Physics* (Saunders College, Philadelphia, PA, 1976), chap. 5.
20. N. W. Ashcroft and N. D. Mermin, *ibid.*, chap. 6.
21. This manuscript is a work of the U.S. government. It is not subject to U.S. copyright. We acknowledge financial support from the Office of Naval Research.

29 August 1997; accepted 14 November 1997

Changes in the West Antarctic Ice Sheet Since 1963 from Declassified Satellite Photography

Robert Bindschadler* and Patricia Vornberger

Comparison of declassified satellite photography taken in 1963 with more recent satellite imagery reveals that large changes have occurred in the region where an active ice stream enters the Ross Ice Shelf. Ice stream B has widened by 4 kilometers, at a rate much faster than suggested by models, and has decreased in speed by 50 percent. The ice ridge between ice streams B and C has eroded 14 kilometers. These changes, along with changes in the crevassing around Crary Ice Rise, imply that this region's velocity field shifted during this century.

One of the major uncertainties in the Intergovernmental Panel on Climate Change's projection of future sea level is the uncertain behavior of the West Antarctic Ice Sheet (*1*). It was much larger during the last glacial maximum 20,000 years ago, and its retreat since then has been rapid at times (*2*). Current behavior does not indicate that it is now retreating rapidly, but areas of rapid change have been discovered and the potential for unstable behavior remains under study.

The thick West Antarctic Ice Sheet is grounded on a submarine bed contained in an extensional rift basin coated with thick marine sediments and is subject to high geothermal heat flow (*3*). Discharge of West Antarctic ice is dominated by rapidly moving ice streams. These ice streams feed floating ice shelves; the transition from grounded to floating ice occurs at the "grounding line." Occasionally ice shelves ground, forming ice rises that the ice shelf must flow around. Between ice streams, the ice accumulates to form higher elevation ridges that slowly flow laterally into the ice streams across heavily crevassed shear margins.

R. Bindschadler, Code 971, NASA–Goddard Space Flight Center, Greenbelt, MD 20771, USA.
P. Vornberger, General Sciences Corporation, 6100 Chevy Chase Drive, Laurel, MD 20727, USA.

*To whom correspondence should be addressed.

Declassified intelligence satellite photography (DISP) recently made available affords a direct view of the ice sheet's configuration in the early 1960s, greatly extending the limited surface observations made during the International Geophysical Year in 1958 to 1959. Here, we analyzed changes in the mouth of ice stream B: from the downstream tip of ridge B/C (between streams B and C) to the area just downstream of Crary Ice Rise (Fig. 1) (*4*).

The DISP data were collected on 29 and 31 October 1963 (*5*). The DISP frames we used were 4 inch by 5 inch (10.16 cm by 12.7 cm) contact negatives, which we scanned at 600 dots per inch to convert them to digital form. They were collected by the cartographic camera onboard a Corona mission satellite and have a ground spatial resolution of about 150 m. Our second data set is a mosaic of two images from the advanced very high resolution radiometer (AVHRR) collected on 12 November 1980 and 8 December 1992. These images were obtained from the U.S. Geological Survey (USGS) World Wide Web site as part of an Antarctic mosaic and have a

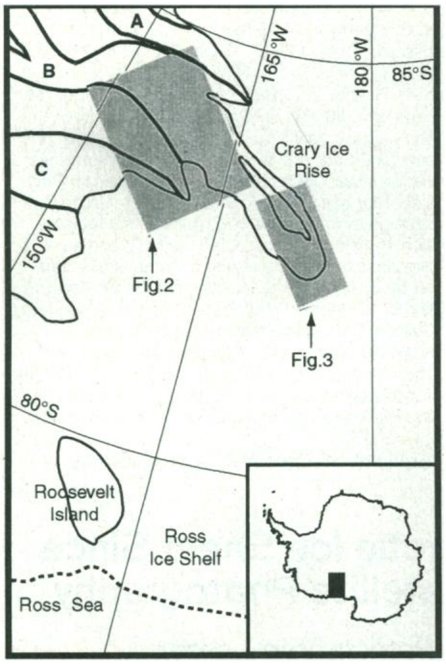

Fig. 1. Location map of study area. Ice streams A, B, and C are shown along with their grounding lines. Shaded areas indicate locations shown in Figs. 2 and 3. Ice flow is generally from upper left toward lower right.

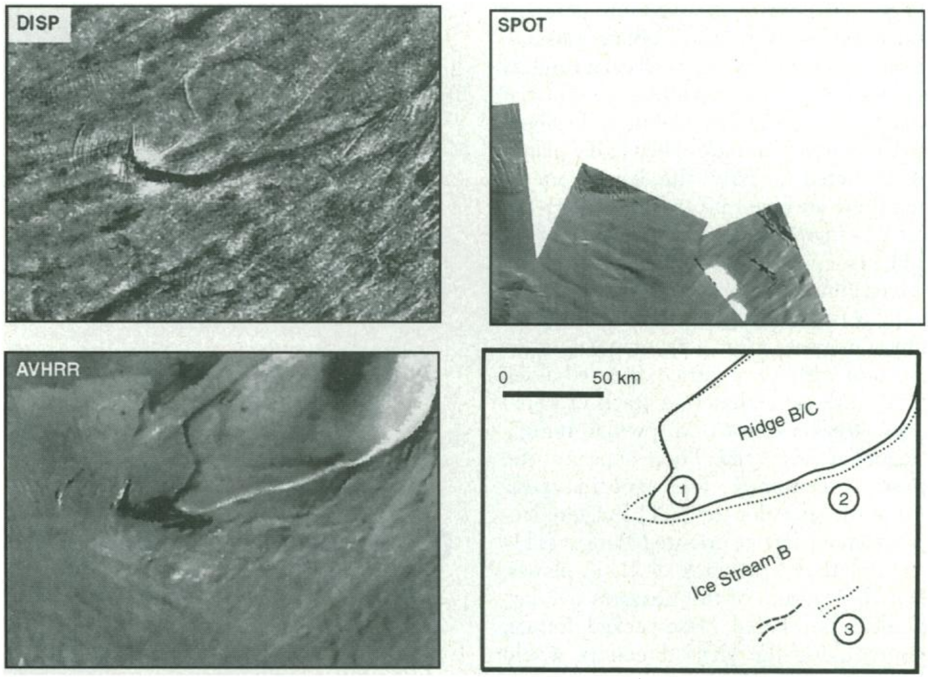

Fig. 2. Co-registered DISP, AVHRR, and SPOT imagery in the vicinity of the mouth of ice stream B. Ice flow is approximately from right to left. (Bottom right) Tracings of particular features from DISP (dotted lines), AVHRR (solid line), and SPOT (dashed lines). Areas identified by circled numbers are discussed in text.

ground spatial resolution of 1100 m (6). Finally, we used a series of panchromatic Satellite Pour l'Observation de la Terre (SPOT) images collected between 23 January 1989 and 12 February 1992 that provide a ground spatial resolution of 10 m (7).

The DISP and AVHRR data were coregistered by locating seven common points circumscribing the study area (one each on Crary Ice Rise and ridge B/C, one at the confluence of ice streams A and B, and four in the Transantarctic Mountains). We applied a two-dimensional linear warping function to the DISP image to match it to the AVHRR imagery. The mean residual of this fit at the control points was 1 km. The SPOT image mosaic was co-registered to the DISP image by using three commonly identifiable points on Crary Ice Rise. The accuracy of the DISP-SPOT co-registration is about 500 m and includes the fact that the SPOT mosaic was made by matching features that may be moving.

The northern side of ridge B/C in the DISP and AVHRR images (SPOT data do not cover the ridge) maintained its shape, but the tip of the ridge retreated 14 km (area 1) and the northern margin of ice stream B (south side of ridge B/C) migrated 4 km (area 2) (Fig. 2).

Erosion of ridge B/C took place at a maximum rate of 447 ± 34 m/year at its tip during the 29.1 years between images. This is considerably faster than the previously measured rate of grounding-line retreat at ice stream C of less than 30 m/year (8). Ice downstream of the tip is likely floating, and the large number of crevasses indicates that the ice is rapidly accelerating as it flows northward (left side of Fig. 2).

The width of an ice stream, in combination with its speed, determines the rate of ice discharge. In contrast to mountain glaciers, which flow within a rock valley, ice streams are bounded by ice. The position of an ice stream margin represents a delicate balance between the advection of cold ice from the ridge into the ice stream (which will tend to narrow and slow the ice stream) and the generation of shear heating within the margin that will warm the ridge ice and tend to widen the ice stream. Recent models of these competing processes have suggested that margins will migrate at rates of from less than 1 m/year to 10 m/year (9).

Our measurement indicates that the margin migrated at an average rate of 137 ± 34 m/year, an order of magnitude faster than models have predicted. This high rate may mean that the advection rate of cold ice was smaller than expected or that the base outside the ice stream was preconditioned to sliding conditions. Repeat measurements of velocity across the margin 300 km upstream have suggested that the margin is widening but at a much slower rate of 10 m/year, which is more in line with models (*10*). Burial depths of an inferred ancient ice stream margin near this upstream site suggest a sustained migration of the margin into the active ice stream at a rate of 100 m/year, beginning 180 years ago and ending 120 years ago (*11*).

If the ice stream's motion is dominated by resistance at the side of the ice stream, an increase in width would produce an increase in speed because the driving force is increased with no increase in resistance. On the other hand, if basal resistance dominates, the speed should not change. As discussed below, the ice stream decelerated, suggesting that other factors are changing as well.

Two flow stripes within the mouth of the ice stream that are associated with a feature known as ice raft A (area 3) are also identified (Fig. 2). This raft is visible on the SPOT imagery as an oval-shaped feature about 15 km long. These form lines maintained their shape from 1963 to 1989 and moved downstream ~20 km. Ice raft A in the SPOT image is more than 150 km from the nearest control point, but because the Crary Ice Rise image and the ice raft A image were acquired less than a year apart, the overall position error in the mosaic is probably less than 500 m. Thus, the average velocity is 770 ± 20 m/year. This is substantially faster than the direct in situ measurement of 471 m/year made between 1984 and 1985 and other in situ measurements made adjacent to ice raft A that confirm this feature has recently moved at the same speed as the surrounding ice stream (to within error) (*12*). If velocity decreased linearly with time, the flow speed in 1963 was 967 m/year, twice the 1984–1985

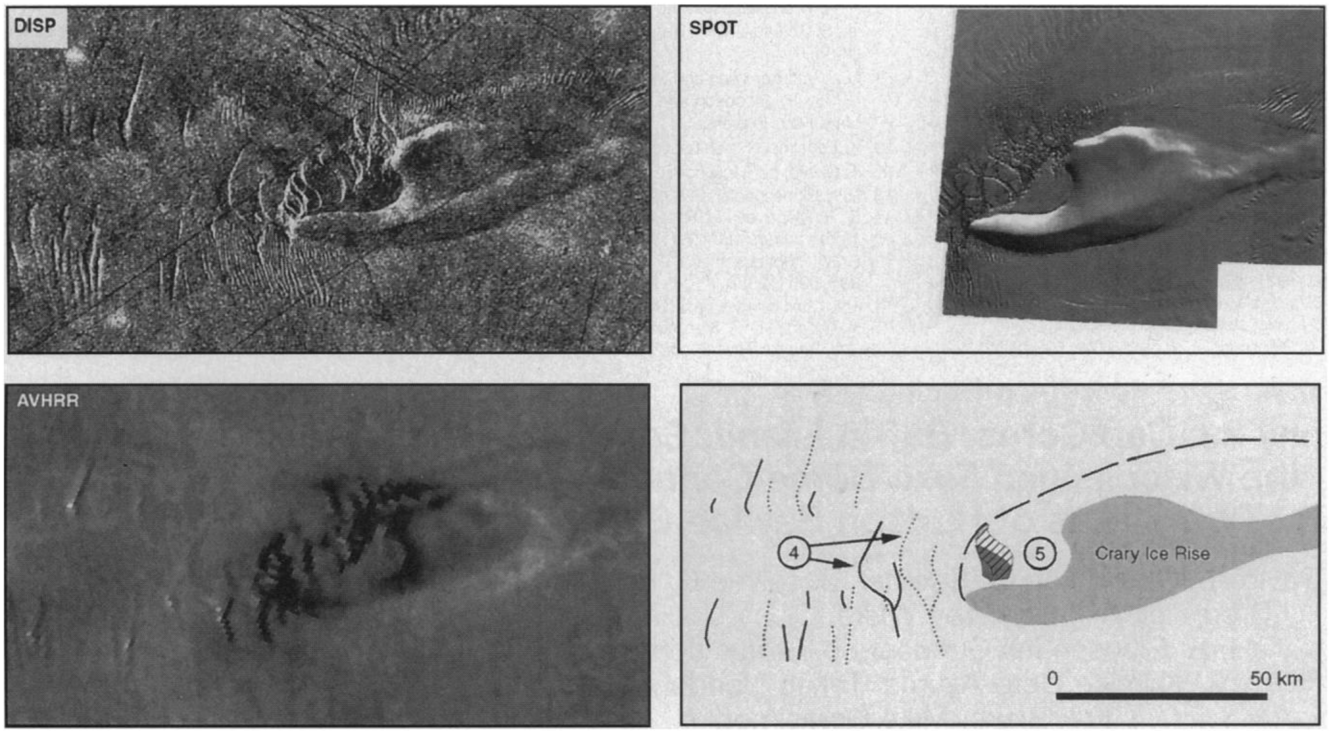

Fig. 3. Co-registered DISP, AVHRR, and SPOT imagery of Crary Ice Rise area. Ice flow is generally from right to left. (Bottom right) Tracings of particular features from DISP (dotted lines), AVHRR (solid lines), and SPOT (dashed line). Areas identified by circled numbers are discussed in text. Lightly shaded area indicates Crary Ice Rise. Hatched and darkly shaded areas indicate positions of a rotated ice block in DISP and SPOT imagery, respectively.

speed. The average rate of deceleration is 2.4% per year, close to the rate of 20% over the decade from the mid-1970s to the mid-1980s inferred by earlier work and significantly extending the duration of this behavior (*13*). Such high rates of change in velocity greatly complicate the calculation of mass balance of the ice sheet when field measurements collected over many years are used.

In the Crary Ice Rise region (flow is toward the left), a succession of crevasses formed by the shearing of ice have moved past either side of the rise. These continue to the edge of the ice shelf 500 km away (Fig. 1) and indicate that the ice rise has been persistent and that it has affected the flow of the ice shelf for more than 800 years (the time required for ice at the rise to reach the shelf front) (*14*). Over this entire distance, the only crevasses occurring between these two separate crevasse trails are the two intersecting crevasses immediately downstream of the ice rise (Fig. 3, arrows point to these crevasses). This pattern indicates that crevassing directly in the lee of the rise is recent. The shape of the most downstream of this joined set, when projected upstream, matches the orientation of the shear crevasses to the southwest of the rise and the curved envelope of the ice rise's shape, suggesting that these crevasses originated at this location. Using the two locations of this crevasse in the 1963 (DISP) and the 1980 (AVHRR) data, the resultant velocity of 590 m/year provides an estimate that the initial formation of these crevasses occurred 21 years before the DISP data (that is, in 1942). A constant acceleration model would double this time estimate to 42 years (in 1921). These dates are close to the 50 years estimated for the time when a large mass of ice separated from the northeastern side of the ice rise (*15*).

Fracturing accompanied the generation of crevasses at the edge of the confined embayment of the ice rise lee (area 5). Many of these same blocks can be identified in the DISP photograph. This comparison (Fig. 3) shows that the blocks are being rotated by the flow of ice past the ice rise. The initial formation of these blocks took place shortly before the 1963 DISP photography. Aerial photography of Crary Ice Rise confirms that crevassing within and extending from the embayment was present by 1947 (*16*). Earlier observations do not exist.

Our analysis demonstrates that this region of the ice sheet has undergone, and continues to experience, large dynamic changes. It is tempting to relate the cause of these events to the shutdown of ice stream C 135 years ago (*17*). It has been suggested that the diversion of subglacial water flow away from ice stream C and toward ice stream B was responsible for ice stream C's sudden termination and an increase in the flow of ice stream B (*18*). This shift in flow would increase the amount of ice passing north and east of Crary Ice Rise, causing increased shear and fracturing of the ice in the formerly protected lee of the ice rise. Arrival at the ice rise's downstream end of flow disturbances generated at the mouth of ice stream C would be delayed by the time it takes the intervening ice to adjust to an altered flow pattern. It is expected that the timing of changes at the ice rise would postdate ice stream C's shutdown.

These observations, although illustrating the dramatic changes that are occurring in one area of West Antarctica, do not resolve the overriding question of the stability of the West Antarctic Ice Sheet. However, the 50% decrease in velocity in less than three decades cannot be explained solely by a slight widening of the ice stream and underscores the fact that large changes in velocity can occur with even small changes to either the external forcings exerted on the ice sheet or its internal dynamics.

REFERENCES AND NOTES

1. *Climate Change 1995, The Science of Climate Change*, J. T. Houghton *et al.*, Eds. (Cambridge Univ. Press, Cambridge, UK, 1996).
2. M. Stuiver, G. H. Denton, T. J. Hughes, J. L. Fastook, in *The Last Great Ice Sheets*, G. H. Denton and T. J. Hughes, Eds. (Wiley-Interscience, New York, 1981), pp. 319–428; B. Hall, thesis, University of Maine (1997).
3. R. B. Alley and I. M. Whillans, *Science* **254**, 959 (1991).

4. Crary Ice Rise is not a true ice rise because it is encompassed by grounded ice. However, the discovery of lightly grounded ice surrounding the ice rise was made after the feature was named.
5. On 22 February 1995, Presidential Executive Order 12951 declassified all intelligence photography collected before 1972 and ordered copies held at both the U.S. Archives and the USGS's Eros Data Center. The USGS operates a Web site–accessible database (http://edcwww.cr.usgs.gov/webglis) for online searches, browse image review, and product ordering.
6. The data available at http://TerraWeb.wr.usgs.gov/TRS/projects/Antarctica/AVHRR have been mapped into a polar stereographic projection.
7. R. A. Bindschadler, *J. Glaciol.* **39**, 538 (1993).
8. R. H. Thomas, S. N. Stephenson, R. A. Bindschadler, S. Shabtaie, C. R. Bentley, *Ann. Glaciol.* **11**, 165 (1988).
9. C. J. Van der Veen and I. M. Whillans, *ibid.* **23**, 129 (1996); P. Jacobson and C. F. Raymond, *J. Geophys. Res.*, in press.
10. K. Echelmeyer, personal communication.
11. T. Clarke, personal communication.
12. R. A. Bindschadler, S. N. Stephenson, E. P. Roberts, D. R. MacAyeal, D. R. Lindstrom, *NASA Technical Memorandum 100708* (1988).
13. S. N. Stephenson and R. A. Bindschadler, *Nature* **334**, 695 (1988).
14. This conclusion is based on published velocities [R. H. Thomas, D. R. MacAyeal, D. H. Eilers, D. R. Gaylord, *Antarct. Res. Ser.* **42**, 21 (1984)].
15. R. A. Bindschadler *et al.*, *Ann. Glaciol.* **11**, 8 (1988).
16. Oblique aerial photographs of Mission 8 examined at the SCAR Library, USGS National Center, Reston, VA.
17. R. Retzlaff and C. R. Bentley, *J. Glaciol.* **39**, 553 (1993).
18. R. B. Alley, S. Anandakrishnan, C. R. Bentley, N. Lord, *Ann. Glaciol.* **20**, 187 (1994).
19. We wish to thank U.S. Vice President Albert Gore and former Central Intelligence Agency Director Robert Gates for initiating the effort that led to the declassification of the photography used in this research. Two anonymous reviewers contributed useful comments. Supported under NSF grant OPP-9616394.

11 November 1997; accepted 15 December 1997

Penny Ice Cap Cores, Baffin Island, Canada, and the Wisconsinan Foxe Dome Connection: Two States of Hudson Bay Ice Cover

David A. Fisher, Roy M. Koerner, Jocelyne C. Bourgeois, Greg Zielinski, Cameron Wake, Claus U. Hammer, H. B. Clausen, N. Gundestrup, Sigfus Johnsen, Kumiko Goto-Azuma, Takeo Hondoh, Erik Blake, Mike Gerasimoff

Ice cores from Penny Ice Cap, Baffin Island, Canada, provide continuous Holocene records of oxygen isotopic composition ($\delta^{18}O$, proxy for temperature) and atmospheric impurities. A time scale was established with the use of altered seasonal variations, some volcanic horizons, and the age for the end of the Wisconsin ice age determined from the GRIP and GISP2 ice cores. There is pre-Holocene ice near the bed. The change in $\delta^{18}O$ since the last glacial maximum (LGM) is at least 12.5 per mil, compared with an expected value of 7 per mil, suggesting that LGM ice originated at the much higher elevations of the then existing Foxe Dome and Foxe Ridge of the Laurentide Ice Sheet. The LGM $\delta^{18}O$ values suggest thick ice frozen to the bed of Hudson Bay.

The Penny Ice Cap on Cumberland Peninsula, Baffin Island, is the southernmost major ice cap in Canada. During the Wisconsin Ice Age, the ice cap was connected to Foxe Dome (*1, 2*) (Fig. 1A). Field evidence suggests that during the Holocene, the position of the central ridge of the thicker southeastern part of the ice cap was stable (*3*). Presently, the central ridge has a maximum surface elevation of 1900 meters above sea level (masl) (Fig. 1B).

D. A. Fisher, R. M. Koerner, J. C. Bourgeois, Terrain Sciences Division, Geological Survey of Canada, 601 Booth Street, Ottawa, Ontario K1A 0E8, Canada.
G. Zielinski and C. Wake, Glacier Research Group, Morse Hall, University of New Hampshire, Durham, NH 03824–3525, USA.
C. U. Hammer, H. B. Clausen, N. Gundestrup, S. Johnsen, Niels Bohr Institute, Department of Geophysics, University of Copenhagen, Rockefeller Complex, Juliane Maries Vej 30, Copenhagen Ø, Denmark DK-2100.
K. Goto-Azuma, Nagaoka Institute of Snow and Ice Studies, 187–16 Suyoshi-machi, Nagaoka-shi, Niigata-ken 940, Japan.
T. Hondoh, Institute of Low Temperature Science, Hokkaido University, Sapporo 060, Japan.
E. Blake and M. Gerasimoff, Icefield Instruments, 3 Glacier Drive, Unit 2, Whitehorse, Yukon Y1A 5H4, Canada.

In spite of relatively high melt (*4*), we established Holocene chronologies for $\delta^{18}O$ and ice chemistry. The proximity of the core to Baffin Bay and the major glaciological changes that occurred during the Holocene make this core an important record. The Wisconsinan ice has sections of low $\delta^{18}O$ and high calcium concentrations. In particular, the episode attributed to the LGM [18 thousand years ago (ka)] suggests origins deep inland on the Foxe Dome and Foxe Ridge of a Laurentide Ice Sheet dominated by Hudson Bay ice frozen to its bed.

Two ice cores 16 km apart reached the bed of the Penny Ice Cap. The 333.78-m P95 core was drilled on the central ridge (1900 masl) (Fig. 1B); we analyzed $\delta^{18}O$, calcium and sodium concentrations, and solid conductivity [electrical conductivity method (ECM)] (Fig. 2). The 177.91-m P96 core was drilled at the top of a separate but joined ice dome (1810 masl) (Fig. 1B); at present, $\delta^{18}O$ and ECM has been measured for P96.

The value of $\delta^{18}O$ (*5*) in precipitation is negative and is related to a site's location in the water cycle (*6, 7*). For high-elevation polar ice masses, the site's air temperature plays a role, as can its elevation. Time series derived from ice-core $\delta^{18}O$ have the flow effect included, whereby older (deeper) ice originated from higher up a flow line, which may have been evolving. Presently, P95 and P96 are close to or at the local highest point (Fig. 1B), so recent ice has local origins in both cores. ECM is a measure of solid-ice conductivity (*8*) and is mainly controlled by pH. Calcium (concentration [Ca^{2+}], measured in nanograms of Ca^{2+} per gram of ice) is mostly from airborne mineral dust, and the sodium (concentration [Na^{+}]) is primarily from sea salt (*9, 10*).

The ice temperature at a depth of 15 m measured by Holdsworth 2 km down-ridge from P95 was −14.4°C (*11*). Under present conditions, the calculated bottom temperature for P95 is −8°C (*12*), so there is little chance that basal melting occurred during the Holocene. At the P95 and P96 sites, 40 and 80% of the accumulation, respectively, melts and refreezes (*4*). The accumulation rate at P95 as determined from the depth of the 1963 bomb layer is 0.37 m (ice equivalent) per year, and the rate determined from the depth of the volcanic layer deposited by the 1783 A.D. Laki event is 0.36 m/year. The Laki-derived accumulation for P96 is 0.188 m/year. At P95, the modern $\delta^{18}O$ is −24.23 per mil; modern $\delta^{18}O$ at P96, however, is −23.37 per mil. There is scouring of winter snow at the P96 site in half of the winters. If the cold (low δ) winters of P95 are numerically removed (*13*), the resulting stratigraphy resembles that for P96 (Fig. 3), and the average δ shifts from −24.23 to −23.5 per mil, which is close to the average for the P96 site. The average accumulation at P95 drops 39% when the deep winters are numerically removed. This sort of episodic scour biases the differences between the sites to the cold δ years (Fig. 4). This episodic scour is different from the more continuous scour seen in drier snow areas (*14*).